NASA/TM-2004-212656

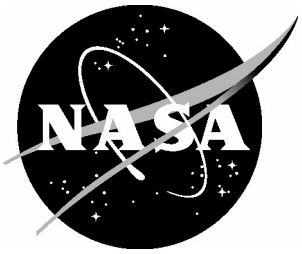

Buckling Behavior of Compression-Loaded Composite Cylindrical Shells With Reinforced Cutouts

Mark W. Hilburger and James H. Starnes, Jr.
Langley Research Center, Hampton, Virginia

September 2004

The NASA STI Program Office . . . in Profile

Since its founding, NASA has been dedicated to the advancement of aeronautics and space science. The NASA Scientific and Technical Information (STI) Program Office plays a key part in helping NASA maintain this important role.

The NASA STI Program Office is operated by Langley Research Center, the lead center for NASA's scientific and technical information. The NASA STI Program Office provides access to the NASA STI Database, the largest collection of aeronautical and space science STI in the world. The Program Office is also NASA's institutional mechanism for disseminating the results of its research and development activities. These results are published by NASA in the NASA STI Report Series, which includes the following report types:

- TECHNICAL PUBLICATION. Reports of completed research or a major significant phase of research that present the results of NASA programs and include extensive data or theoretical analysis. Includes compilations of significant scientific and technical data and information deemed to be of continuing reference value. NASA counterpart of peer-reviewed formal professional papers, but having less stringent limitations on manuscript length and extent of graphic presentations.

- TECHNICAL MEMORANDUM. Scientific and technical findings that are preliminary or of specialized interest, e.g., quick release reports, working papers, and bibliographies that contain minimal annotation. Does not contain extensive analysis.

- CONTRACTOR REPORT. Scientific and technical findings by NASA-sponsored contractors and grantees.

- CONFERENCE PUBLICATION. Collected papers from scientific and technical conferences, symposia, seminars, or other meetings sponsored or co-sponsored by NASA.

- SPECIAL PUBLICATION. Scientific, technical, or historical information from NASA programs, projects, and missions, often concerned with subjects having substantial public interest.

- TECHNICAL TRANSLATION. English-language translations of foreign scientific and technical material pertinent to NASA's mission.

Specialized services that complement the STI Program Office's diverse offerings include creating custom thesauri, building customized databases, organizing and publishing research results ... even providing videos.

For more information about the NASA STI Program Office, see the following:

- Access the NASA STI Program Home Page at ***http://www.sti.nasa.gov***

- E-mail your question via the Internet to help@sti.nasa.gov

- Fax your question to the NASA STI Help Desk at (301) 621-0134

- Phone the NASA STI Help Desk at (301) 621-0390

- Write to:
  NASA STI Help Desk
  NASA Center for AeroSpace Information
  7121 Standard Drive
  Hanover, MD 21076-1320

NASA/TM-2004-212656

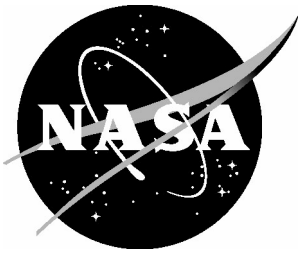

Buckling Behavior of Compression-Loaded Composite Cylindrical Shells With Reinforced Cutouts

Mark W. Hilburger and James H. Starnes, Jr.
Langley Research Center, Hampton, Virginia

National Aeronautics and
Space Administration

Langley Research Center
Hampton, Virginia 23681-2199

September 2004

Available from:

NASA Center for AeroSpace Information (CASI)
7121 Standard Drive
Hanover, MD 21076-1320
(301) 621-0390

National Technical Information Service (NTIS)
5285 Port Royal Road
Springfield, VA 22161-2171
(703) 605-6000

Abstract

Results from a numerical study of the response of thin-walled compression-loaded quasi-isotropic laminated composite cylindrical shells with unreinforced and reinforced square cutouts are presented. The effects of cutout reinforcement orthotropy, size, and thickness on the nonlinear response of the shells are described. A nonlinear analysis procedure has been used to predict the nonlinear response of the shells. The results indicate that a local buckling response occurs in the shell near the cutout when subjected to load and is caused by a nonlinear coupling between local shell-wall deformations and in-plane destabilizing compression stresses near the cutout. In general, reinforcement around a cutout in a compression-loaded shell is shown to retard or eliminate the local buckling response near the cutout and increase the buckling load of the shell. However, some results show that certain reinforcement configurations can cause an unexpected increase in the magnitude of local deformations and stresses in the shell and cause a reduction in the buckling load. Specific cases are presented that suggest that the orthotropy, thickness, and size of a cutout reinforcement in a shell can be tailored to achieve improved buckling response characteristics.

Introduction

The high performance requirements of future aerospace structures and the projected increase in airtravel and space access require the development of more efficient aerospace structures. The high strength-to-weight and high stiffness-to-weight ratios of advanced composite materials offer significant weight reduction potential for aerospace structures. In addition, the use of advanced composite materials allows the designer to tailor the stiffness properties of the structure to obtain a structurally efficient design.

Thin-walled cylindrical shells are found in many aerospace structural applications because of their high load carrying capacity and low structural weight. Many of these aerospace shell structures have cutouts or openings that serve as doors, windows, or access ports and these cutouts or openings often require some type of reinforcing structure to control local structural deformations and stresses near the cutout. In addition, these structures may experience compression loads during operation, and thus their buckling and postbuckling response characteristics must be understood and accurately predicted in order to determine effective designs and safe operating conditions for these structures.

Many studies have been conducted which show that a cutout in an isotropic shell structure can have a significant effect on the response of the shell. In particular, results indicate that a cutout in a shell structure causes a local response to occur near the cutout when the shell is subjected to load. This local response can consist of large out-of-plane deformations and large-magnitude, rapidly varying stresses near the cutout (e.g., Refs. 1-2). If the applied load is a compressive load, the cutout can cause a local buckling response to occur in the shell at applied load levels lower than the general instability load of the corresponding shell without a cutout (e.g., Refs. 3-5). For some cases, this local buckling response results in a stable postbuckling response localized near the cutout and additional load can be applied to the shell

before it exhibits global collapse. For other cases, the local response in the shell causes a disturbance in the shell of sufficient magnitude to cause global collapse to occur immediately after the local instability occurs.

Relatively few studies have been conducted on the effects of a cutout on the response of a compression-loaded composite cylindrical shell. Recent numerical and experimental studies of the response of compression-loaded composite cylindrical shells with unreinforced rectangular cutouts have been presented by Hilburger, et al.[6, 7] Their results show that localized regions of biaxial in-plane compression stresses form in the shell near the cutout, and these regions of biaxial stresses couple with the out-of-plane deformations of the shell wall causing an unstable local buckling response to occur near the cutout. In addition, their results indicate that laminate orthotropy can have a significant effect on the nonlinear response and the buckling behavior of a shell with a cutout. Similarly, very few studies have been conducted on the response of compression-loaded curved shells with reinforced cutouts, and the few results that do exist are limited to isotropic shells (e.g., Refs. 8-10). Almroth and Holmes[8] presented results from a numerical and experimental study on the response of compression-loaded cylindrical shells with reinforced and unreinforced rectangular cutouts. Their results show that the arrangement of the cutout reinforcement, that is, whether the reinforcement is positioned along the axially aligned free-edges of the cutout or around all of the edges of the cutout, can have a significant effect on the buckling response of the shell. Experimental results from Toda[10] indicate that, for certain sized circular cutouts in a compression-loaded cylindrical shell, the bucking load increased with an increase in the size of the reinforcement around the cutout. However, further reinforcement of the cutout beyond a certain amount did not always produce higher buckling loads, and in some cases, further reinforcement caused a decrease in the buckling load of the shell. Unfortunately, no detailed explanation of this interesting behavioral characteristic was given in the paper by Toda.

The traditional method for the preliminary design of a reinforced cutout in a thin-walled shell structure is based on a linear analysis of a flat plate with a square cutout (e.g., Ref. 11). The effects of shell curvature and other modeling approximations are taken into account by applying empirical correction factors. However, this design method may not be sufficient for the design of large reinforced cutouts in curved shell structures because of the complex nonlinear behavior exhibited by these types of structures. In addition, this design method can result in overly conservative designs or unconservative designs for these structures if the empirical correction factors are not applicable to the design of interest. For example, current design guides do not address the design of reinforced cutouts in stability-critical composite shell structures.

A review of the results presented in the literature indicates that the response of a compression-loaded cylindrical shell with an unreinforced cutout is, for the most part, understood. In contrast, the effects of cutout reinforcement on the buckling behavior of compression-loaded composite cylindrical shells, is not well understood. The objective of the present paper is to identify typical nonlinear response characteristics of a compression-loaded, thin-walled, quasi-isotropic, laminated, cylindrical shell with a square cutout and to illustrate the effects of several cutout reinforcement configurations on the response. Toward this objective, numerically predicted results that show the effects of 18 different reinforcement configurations on the response of these shell structures are presented. The cutout reinforcement configurations considered were used to study the effects of reinforcement orthotropy, thickness, and size on the response of the shell. In addition, the results are used to illustrate the feasibility of structurally tailoring cutout reinforcement to control shell-wall deformations and stress concentrations near a cutout in a compression-loaded shell, and to increase the load carrying capacity of the shell. The thin-walled cylindrical shell configuration presented herein was chosen as a generic example of a typical aerospace shell structure with a cutout and subjected to a destabilizing load. A modern high-fidelity nonlinear

analysis procedure is used in the study (e.g., Ref. 12). This high-fidelity analysis procedure has been successfully applied to the analysis of other similar compression-loaded shells with cutouts, and the predicted results have been verified with selected experiments, e.g., see Ref. 7. This procedure offers the opportunity to provide insight into the effects of various cutout reinforcement concepts on the response of compression-loaded shell structures and to improve some of the engineering approximations and methods that are used in the design of reinforced cutouts in shell structures. First, the finite-element models and analysis procedures are described. Next, results illustrating the response of a compression-loaded cylinder with an unreinforced cutout are presented. Then, results illustrating the effects of selected cutout reinforcement on the response of the shell are presented. Lastly, response trends are identified and discussed. The results include load-shortening response curves, prebuckling, buckling and postbuckling deformation patterns, and prebuckling, buckling, and postbuckling stress contours.

Finite-Element Models and Analyses

Finite-Element Models

The nineteen shells considered in this study were analyzed with the STAGS (STructural Analysis of General Shells) nonlinear shell analysis code.[13] A typical finite-element model of a shell with a centrally located square cutout is shown in Fig. 1. The shells have a length L of 16.0 in., a radius R of 8.0 in., and shell-wall thickness t of 0.04 in. giving a shell-radius-to-thickness ratio of 200. A 1.0-in. by 1.0-in. square cutout with 0.05-in-radius reentrant corners is located at $\theta = 0^{\circ}$ and at the shells mid-length. The shells were modeled as geometrically perfect, 8-ply-thick $[\pm 45/0/90]_s$ quasi-isotropic graphite-epoxy laminates, in which each lamina ply had a thickness of 0.005 in. and a fiber volume fraction of 0.62. The lamina material properties are as follows: longitudinal compression modulus $E_1 = 18.5$ Msi, transverse modulus $E_2 = 1.64$ Msi, in-plane shear modulus $G_{12} = 0.87$ Msi, and major Poisson's ratio $\nu_{12} = 0.30$. The shells were analyzed in the present study and include one shell with an unreinforced cutout and 18 shells with reinforced cutouts. These shells are referred to herein as shells C1 through C19. The cutout reinforcement consists of additional square-shaped lamina plies added to the shell-wall laminate at the shell-wall mid-surface that are aligned concentrically with respect to the square-shaped cutout in the shell. Eighteen different reinforcement configurations were considered in which the reinforcement thickness, size, and ply-orientation were varied. Specifically, three different reinforcement thicknesses of 0.005 in., 0.01 in., and 0.02 in., corresponding to one, two, and four-ply reinforcement thicknesses, respectively, were considered. Two reinforcement ply orientations of 0º and 90º were investigated (a 0º ply and a 90º ply correspond to lamina plies with fibers aligned along the length of the shell and around its circumference, respectively) to study the effects of reinforcement orthotropy on the response. Three square-shaped reinforcement sizes included a 2.4-in. by 2.4-in. square reinforcement, a 4.4-in. by 4.4-in. square reinforcement, and a 8.0-in. by 8.0-in. square reinforcement (referred to herein as 2.4-in-square reinforcement, 4.4-in- square reinforcement, and 8.0-in-square reinforcement, respectively). A list of shell identification codes and corresponding reinforcements are given in Table 1.

The shells were modeled using standard 410 quadrilateral element from the STAGS element library. The element is a flat facet-type element that is based on the Kirchoff-Love shell theory and the nonlinear Lagrangian strain tensor. The element nodes each have three translational degrees of freedom, u, v, w, and three rotational degrees of freedom about the x, θ, and z axis. Large element rotations are accounted for by using a co-rotational algorithm. The elements of the finite-element mesh are typically approximately 0.2-in. by 0.2-in. square, with increased mesh refinement near the cutout. Each element possesses four integration points in the plane, which are distributed to provide a modeling resolution of at least 0.1-in. Results from a mesh convergence study indicated that this degree of mesh refinement was required to accurately model the bending boundary layer deformation response near the ends of the shell,

the prebuckling short wavelength deformation response and rapidly varying stress distributions exhibited by the shells near the cutout, and the short wavelength deformation response and rapidly varying stress distributions exhibited by the shells during the transient buckling process. Clamped end conditions were simulated in the finite-element models by setting the circumferential and radial displacements v and w equal to zero in the 1.0-in-long end regions of the shell, as indicated in Fig. 1. A typical finite-element model contained approximately 120,000 degrees of freedom.

Nonlinear Analysis Procedure

The STAGS code is designed for the static and dynamic analysis of general shells, and includes the effects of geometric and material nonlinearities in the analysis. The STAGS code uses both the modified and full Newton methods for its nonlinear solution algorithms, and accounts for large rotations in a shell wall by using a co-rotational algorithm implemented at the element level. The Riks pseudo arc-length path-following method[14] is used to continue a solution past the limit points of a nonlinear response. With this strategy, the incrementally applied loading parameter is replaced by an arc-length along the solution path, which is then used as the independent loading parameter. The arc-length increments are automatically adjusted by the program as a function of the solution behavior. A transient analysis option is included in STAGS that uses an implicit numerical time-integration method developed by Park[15] and proportional structural damping. Mass and stiffness damping factors used in the transient analysis are defined as $\alpha = 2\pi\nu\zeta$, and $\beta = \zeta/2\pi\nu$, respectively, where ζ denotes the fraction of critical damping and is assumed to equal 0.15 for the shells considered in the present study. The dynamic buckling response of a shell is assumed to be dominated by a particular frequency of vibration n and is defined as the fundamental frequency of vibration determined from a linear vibration analysis in STAGS. Additional information on the transient analysis in STAGS can be found in Ref. 16. It should be noted that using different damping parameters in the analysis can have an effect on the predicted transient buckling response of the shell. Results from a limited numerical parametric study on the effects of damping on the transient buckling response of the shells indicate that variations in the damping parameters can affect the solution path between the stable prebuckling state and the stable postbuckling state. However, for the damping parameters considered in this study, the overall character of the transient response of the shells remains similar and variations in the damping parameters do not affect the static postbuckling solution. For problems in which path dependence is important such as progressive failure analysis or strain rate dependent materials, variations in the damping parameters may have an effect on the results.

The prebuckling, buckling and postbuckling responses of the shells were determined by using the following analysis procedure. The quasi-static responses were determined by using the geometrically nonlinear quasi-static analysis capability in STAGS. The Riks arc-length path-following method was used to compute the response of the shell up to the buckling point. The unstable buckling response of the shell was predicted by using the nonlinear transient analysis option of the code. The transient analysis was initiated from an unstable equilibrium state close to the buckling point by incrementing the end displacement by a small amount, approximately 1%. An initial time step of 10^{-8} seconds was used in the analysis and is automatically adjusted by the program as a function of the solution behavior. The transient analysis was continued until the kinetic energy in the shell dissipated to a negligible level, which indicates that the transient response has attenuated. Once the transient analysis had attenuated to a near-steady-state solution, the load relaxation option of the code was used to establish a stable static equilibrium state. Conventional linear bifurcation buckling analysis results were also determined with STAGS for comparison with the nonlinear analysis results.

Results and Discussion

Numerically predicted results for selected compression-loaded quasi-isotropic laminated cylindrical shells with unreinforced and reinforced cutouts are presented in this section. The results were obtained from finite-element models of geometrically perfect shells subjected to a uniform axial end-shortening. These results are presented to illustrate the overall behavior of a compression-loaded graphite-epoxy shell with a cutout and the effects of cutout reinforcement on the response. First, results illustrating the nonlinear response of a compression-loaded geometrically perfect quasi-isotropic cylindrical shell with an unreinforced square-shaped cutout are presented. Then, results illustrating the predicted response of selected compression-loaded cylindrical shells with reinforced cutouts are presented and compared. The results include load-shortening response curves, prebuckling, buckling and postbuckling deformation patterns, and prebuckling, buckling, and postbuckling stress contours.

Cylindrical Shell with an Unreinforced Cutout

Results for a quasi-isotropic shell with a 1.0-in by 1.0-in unreinforced square-shaped cutout, referred to herein as shell C1, are presented in this section to illustrate typical response characteristics of a compression-loaded shell with a square cutout. The numerically predicted load-shortening response curve for shell C1 is shown in Fig. 2a. The quasi-static responses are indicated by solid lines and the unstable, transient buckling responses are indicated by the dashed lines in the figure. The axial load P is normalized with respect to the bifurcation buckling load predicted from a linear eigenvalue analysis of the corresponding shell without a cutout, P_{cr} = 42,590 lbf, and the end-shortening displacement Δ is normalized with respect to the shell length, L. The shell exhibits a complex nonlinear response as indicated by the numerous stable and unstable segments of the load-shortening response curve. Specifically, the shell has a linear prebuckling response and a distinct buckling point labeled **A** at a load level of P/P_{cr} = 0.51. The buckling response is characterized by a localized, unstable dynamic buckling response in the shell and includes the formation of large magnitude radial deformations and rapidly varying stresses in the shell wall near the cutout. The shell exhibits a relatively small reduction in axial load during buckling and is equal to approximately 6% of the critical load. The load reduction is indicated by the dashed line-segment **A-B** of the load-shortening response curve. The quasi-static solution path from point **A** to point **B** that was predicted by using the arc-length path-following method is also shown in the figure. The results indicate that the quasi-static analysis and the transient analysis predict the same postbuckling deformation and stress states at point **B**. During the prebuckling response, regions of destabilizing in-plane biaxial compression stresses form near the cutout and couple with the radial deformations near the cutout to cause the unstable local buckling response in the shell. A stable postbuckling response is exhibited by the shell, as indicated by segment **B-C** of the load-shortening response. As loading continues in the postbuckling region of the response, the magnitude of the shell-wall radial deformations near the cutout increases. In addition, the results indicate that a significant reduction in the effective axial stiffness of the shell occurs in the postbuckling range of loading. This decrease in effective axial stiffness is caused by increasingly large radial deformations that develop in the shell that cause a significant redistribution of load away from the cutout, there by reducing the effective, load-carrying cross-section of the shell. The global collapse of the shell occurs at point **C** and the unstable collapse response is represented in Fig. 2a by the dashed line segment **C-F**. The collapse response is characterized by a significant reduction in axial load and the development of the general instability deformation pattern. The transient nature of the unstable buckling response in the shell is indicated by the load-time history of the collapse response of the shell shown in Fig. 2b. The load history curve exhibits a sudden reduction in axial load supported by the shell from P/P_{cr} = 0.51, at time t = 0.0 seconds, to P/P_{cr} = 0.32, at time t = 0.006 seconds into the transient response. In addition, the kinetic energy in the shell increases rapidly during the initial collapse response and then dissipates as time

progresses until the shell reaches a stable postbuckling equilibrium configuration. The shell obtains a stable postbuckling configuration after approximately 0.015 seconds have elapsed and the normalized postbuckling load value for the shell is equal to 0.33.

Deformation patterns corresponding to selected points during the compression response are shown in Figs. 3a-3f, and deformation patterns with superimposed axial and circumferential stress contours corresponding to selected points during the compression response are shown in Figs. 4a-4c (the magnitude of the deformation responses in these figures is exaggerated for clarity). The deformation response incipient to local buckling, (associated with point **A** in Fig. 2a), is shown in Fig. 3a, and is characterized by two ellipse-shaped inward buckles near the cutout with the semi-major axis of the buckles aligned in a helical or skew direction. The magnitude of the shell-wall radial deformations vary between -0.65 and +0.40 times the shell-wall thickness, where positive- and negative-valued displacements correspond to outward and inward radial displacements, respectively. The skewing of the deformation pattern is attributed to the presence of laminate anisotropy in the form of coupling between the bending and twisting of the shell wall. The axial and circumferential membrane stress contours indicate significant stress concentrations near the cutout that rapidly decay to far-field values away from the cutout, as shown in Fig. 4a (magnified frontal views of the stresses near the cutout are shown for clarity). The maximum value of the axial compression stress resultant occurs at the corners of the cutout (-2023 lb/in.) and is equal to 4.7 times the corresponding uniform far-field value. Similarly, large magnitude circumferential stress concentrations occur near the cutout with stress resultant values that range between -695 lb/in. and +528 lb/in, the maximum circumferential tension stress resultant occurs at the mid-point of the upper and lower free-edges of the cutout and the maximum circumferential compression stress resultant occurs at the cutout corners. In addition, regions of localized circumferential compression stress develop approximately 0.5 inches above and below the cutout with maximum stress levels of approximately -110 lb/in. The local buckling response of the shell is initiated by a nonlinear coupling between localized destabilizing compressive axial and circumferential stress resultants and the radial deformations that occur in the shell near the cutout. The locations where local buckling initiates are marked by **X** symbols in Fig. 4a. The initial postbuckling deformation pattern associated with point **B** in Fig. 2a is shown in Fig. 3b and is characterized by large ellipse-shaped buckles on either side of the cutout. The magnitude of the shell-wall radial deformations have increased significantly and vary between -4.5 and +1.5 times the shell-wall thickness. As loading continues in the postbuckling range, the ellipse-shaped buckles in the shell wall increase in size and the buckle pattern rotates clockwise around the cutout, as shown in Fig. 3c. The magnitude of the shell-wall radial deformations increases to between -8.65 and +4.2 times the shell-wall thickness and a significant redistribution of the load in the shell occurs near the buckles, as shown in Fig. 4b. More specifically, the axial stress resultant distribution indicates a significant unloading of the shell near the inward buckles. This load redistribution coincides with the reduction in postbuckling stiffness indicated in Fig. 2a and causes a reduction in the effective, load-carrying cross-section of the shell. Moreover, a significant increase in the magnitude of the circumferential compression stress resultants occurs in the buckles. At the onset of global collapse, the shell-wall deformations change in a very short period of time from the stable, local deformation pattern shown in Fig. 3c to an unstable transient deformation pattern shown in Fig. 3d. Additional buckles form in the shell wall around the circumference of the shell. As the buckling process continues, even more buckles develop in the shell wall and the axial load is significantly reduced, as indicated in Fig. 3e. After approximately 0.015 seconds have elapsed, the kinetic energy in the shell has dissipated to a negligible level, and the shell has deformed into a stable post-collapse general instability mode-shape that consists of eight buckles distributed around the circumference of the shell as shown in Fig. 3f. The corresponding post-collapse axial and circumferential stress resultant distribution patterns are shown in Fig. 4c and indicate significant stress resultant redistribution throughout the entire shell. In particular, the results indicate that the majority of the applied axial compression load is now supported by the ridges between

the adjacent inward buckles in the shell wall, and alternating bands of circumferential tension and compression stress resultants are present in the shell.

Cylindrical Shell with a Reinforced Cutout

The buckling results for the compression-loaded shell C1 with an unreinforced cutout, presented in the previous section, identified several features of the nonlinear behavior that are associated with the local buckling response of the shell. Most significantly, the nonlinear interaction between localized radial deformations and destabilizing biaxial stresses near the cutout cause the local buckling response to occur. This fundamental behavioral characteristic suggests that it may be possible to retard or eliminate the onset of the local buckling response near the cutout if a cutout reinforcement configuration can be identified that retards the onset of either or both of the localized deformations and destabilizing stress near the cutout. Thus, a numerical parametric study was conducted to identify the effects of selected cutout reinforcement configurations on the response of a shell with a cutout. In particular, cutout reinforcement size, thickness, and orthotropy were studied. All of the reinforcements considered herein consist of square-shaped concentrically aligned lamina plies added to the shell-wall laminate at the shell-wall mid-surface. Three reinforcement sizes were investigated to identify the effects of reinforcement size on the deformation response and stress distribution in the shell. The three square-shaped reinforcement sizes include 2.4-in. by 2.4-in, 4.4-in. by 4.4-in, and 8.0-in by 8.0-in square reinforcement. Three reinforcement thicknesses were studied and include reinforcement thickness equal to 0.005 in., 0.01 in., and 0.02 in., corresponding to one-, two-, and four-ply reinforcements, respectively. Two reinforcement ply orientations of 0º and 90º (a 0º-ply and a 90º-ply correspond to lamina plies with fibers aligned along the length of the shell and around its circumference, respectively) were investigated to study the effects of reinforcement orthotropy on the response. A list of shell identification codes and corresponding reinforcement configurations is given in Table 1.

Selected results for eighteen compression-loaded quasi-isotropic shells C2-C19 with 1.0-in.-square reinforced cutouts are presented in this section to identify the effects of selected cutout reinforcement configurations on the response of the shells. The results for these shells are compared to results for the corresponding shell C1 with an unreinforced cutout. Results illustrating the effects of cutout reinforcement thickness and orthotropy on the typical response characteristics and response trends for compression-loaded shells with a 4.4-in.-square cutout reinforcement configuration are presented first. Results summarizing the effects of cutout reinforcement area, thickness, and orthotropy on the buckling load and stress resultants of a shell with a reinforced cutout are presented next. Finally, results indicating some bending boundary layer interaction effects are presented and discussed.

4.4-in. Square Reinforcement Results for shells C8 through C13 are presented in this section. The cutout reinforcements for shells C8 through C10 consist of 4.4-in square-shaped 0º lamina plies and the cutout reinforcements for shells C11 through C13 consist of 4.4-in square-shaped 90º lamina plies. Shells C8 and C11 have 0.005-in-thick reinforcement, shells C9 and C12 have 0.01-in-thick reinforcement, and shells C10 and C13 have 0.02-in-thick reinforcement. Numerically predicted load-shortening response curves for shells C8 through C10 and shells C11 through C13, are presented in Figs. 5a and 5b, respectively. The quasi-static responses are indicated by the solid lines and the unstable, transient buckling responses are indicated by the dashed lines in the figure. The axial load P is normalized with respect to the bifurcation buckling load of the corresponding shell without a cutout P_{cr} = 42,590 lbf, and the end-shortening Δ is normalized with respect to the shell length L. The local buckling points are marked with filled circles, and global collapse points are indicated by an **X** on the figure. Curves showing the unstable transient responses associated with local buckling (e.g., line segment **A-B** shown in Fig. 2a for shell C1) for shells C1 and C8 are omitted from Figs. 5a and 5b for clarity. The

results in Figs. 5a and 5b show that the addition of reinforcement around the cutout can have a significant effect on the overall character of the response of the shell. In particular, the local buckling loads increase significantly as the thickness of the reinforcement increases. Specifically, the normalized buckling loads for shells C8, C9, and C10 with 0º-ply reinforcement are equal to 0.62, 0.73, and 0.84, respectively, as compared to the normalized buckling load of 0.51 for the corresponding unreinforced shell C1. Similarly, the normalized buckling loads for shells C11, C12, and C13 with 90º-ply reinforcement are equal to 0.64, 0.76, and 0.92, respectively. These results indicate that the shells with 90º-ply reinforcements considered here exhibit higher buckling loads than the corresponding buckling loads of shells with 0º-ply reinforcements, more specifically, the buckling loads for shells C11, C12, and C13 are 3.2, 4.1, and 9.5% higher than for shells C8, C9, and C10, respectively. In addition, the results indicate that some of the shells with thicker reinforcement, shells C9-C13, do not have stable post-local-buckling responses. For these shells, the local buckling response in the shell causes a disturbance of sufficient magnitude to cause the global collapse of the shell. This response characteristic is in contrast to that of shell C8, which has a stable post-local-buckling response before global collapse occurs, similar to that of shell C1 (see Fig. 2a). After global collapse occurs, each shell has a stable post-collapse configuration, accompanied by a significant reduction in the axial load. The normalized post-collapse loads range from 0.31 to 0.35, and these post-collapse loads are similar to that of the corresponding shell C1 with an unreinforced cutout.

Displacement contour patterns just before buckling for shells C8-C10 with 0º-ply reinforcements are shown in Figs. 6a-6c, respectively. The radial displacements w are normalized by the nominal shell-wall thickness t = 0.04 in. The outer boundary of the cutout reinforcement in each shell is marked in the figures with solid lines. In general, the results indicate that the character of the deformation patterns, just before local buckling occurs, can change significantly as the thickness of the reinforcement increases. In addition, the magnitude of the local deformations near the cutout decreases as the thickness of the reinforcement increases. The displacement contour pattern for shell C8, shown in Fig. 6a, has a large-magnitude local deformation response that rapidly attenuates away from the cutout in a manner similar to that of shell C1. This pattern is characterized by two ellipse-shaped inward buckles near the cutout. The semi-major axis of the buckles is aligned in a helical direction and the localized displacement gradients rapidly attenuate away from the cutout. The magnitude of the normalized shell wall deformations range from -0.47 to 0.35 for shell C8, compared to -0.65 to 0.4 for shell C1, and correspond to as much as a 28% reduction in the magnitude of the local deformations near the cutout compared to shell C1. The character and the magnitude of these local deformations change significantly as the thickness of the reinforcement increases as shown in Figs. 6b and 6c. For example, the normalized displacement magnitudes range from 0.37 to 0.57 near the cutout for shell C10 and correspond to a 81% reduction in the magnitude of the displacement gradient near the cutout (see Fig. 6c). However, large-magnitude displacements exist away from the cutout, and the shell can have normalized displacement values as large as -0.40, as shown in Fig. 6c. Furthermore, the displacement attenuation lengths increase around the circumference of the shell as the reinforcement thickness increases.

The character of the local axial and circumferential stress resultant distributions just before buckling for shells C8 and C9 is similar to the character of the local stress resultant distribution predicted for shell C1 shown in Fig. 4a. However, the magnitudes of the stress resultants can vary significantly as the thickness of the cutout reinforcement increases. The magnitudes of the axial and circumferential stress resultants in the regions of biaxial compression just before buckling are N_x = -719 lb/in and N_θ = -129 lb/in for shell C8, and N_x = -865 lb/in. and N_θ = -126 lb/in. for shell C9 compared to N_x = -568 lb/in. and N_θ = -110 lb/in. for shell C1 (locations of the biaxial compression stress are marked with an **X** symbol in Fig. 6). For comparison purposes, an axial stress concentration factor and a biaxial-stress ratio is defined. The axial stress concentration factor is defined as the local axial stress resultant value in the region of biaxial stress N_x normalized by the far-field value of axial stress resultant $N_x^o = P/2\pi R$, where P is the

axial load applied to the shell and R is the shell radius. The biaxial-stress ratio N_θ / N_x is defined as the ratio of the local circumferential stress resultant to the local axial stress resultant in the region of biaxial compression. These stress resultants in the region of biaxial compression correspond to axial stress concentration factors of 1.36 and 1.40 for shells C8 and C9, respectively, compared to 1.31 for shell C1, and to biaxial-stress ratios of 0.18 and 0.15 for shells C8 and C9, respectively, compared to 0.19 for shell C1. However, the axial and circumferential stress resultant distributions change significantly as the thickness of the reinforcement increases further. Specifically, shell C10 has localized regions of in-plane biaxial compression stress resultants in the bending boundary layer regions near the ends of the shell, and the magnitudes of the stress resultants are N_x = -985 lb/in. and N_θ = -58 lb/in. These stress resultants correspond to an axial stress concentration factor of 1.38, and a biaxial-stress ratio of 0.06. Locations of the biaxial compression stress for this shell are marked with an **X** symbol in Fig. 6c.

The deformation and stress resultant patterns indicate that the initiation and overall character of the local buckling responses of shells C8 and C9 are similar to that of shell C1. The local buckling response in shells C8 and C9 initiates near the cutout and is caused by a nonlinear coupling of the localized regions of destabilizing in-plane biaxial compression stress resultants and the local radial shell-wall deformations. Buckling initiates in shells C8 and C9 at locations that are within the reinforced region of the shells, as indicated with an **X** symbol in Figs. 6a and 6b. As the thickness of the reinforcement is increased further, the shells do not exhibit a local buckling response near the cutout, e.g., shell C10. For this case, a local buckling response initiates in the bending boundary layer regions near the ends of the shell where large-magnitude inward deformations occur. The locations where the buckling initiates in shell C10 are marked with an **X** symbol in Fig. 6c. These deformations couple with localized destabilizing in-plane biaxial compression stress resultants in the bending boundary layer region of the shell. This localized buckling response in the bending boundary layer region causes global collapse to occur. This result illustrates how the reinforcement configuration thickness can have a significant effect on the character of the buckling response. In particular, the cutout reinforcement in shell C10 suppresses the local buckling response near the cutout, and a different localized response in the bending boundary layer region causes the shell to buckle.

The normalized deformation responses just before buckling for shells C11-C13 with 90º-ply reinforcements are shown in Figs. 7a-7c, respectively. The results shown in Fig. 7 illustrate that for shells with 90º-ply reinforcement, the reinforcement thickness can have a significant effect on the deformation response, as was demonstrated for the shells with the 0º-ply reinforcement. The normalized radial displacement contour patterns just before buckling for shells C11 and C12 are characterized by local large-magnitude deformations that rapidly attenuate away from the cutout and are similar to the radial displacement contours of shell C1. The magnitudes of the shell-wall deformations increase with the addition of the cutout reinforcement; specifically, the magnitudes of the shell-wall deformations range between -0.67 to 0.39 for shell C11 and between -0.96 to 0.68 for shell C12, compared to -0.65 to 0.4 for shell C1. These results correspond to an increase in the magnitude of the displacements by as much as 70% in shells C11 and C12 and this response trend is in contrast to that of the corresponding shells with a 0º-ply reinforcement configuration. However, shell C13, which has a thicker reinforcement than shells C11 and C12, exhibits significant differences in its deformation pattern compared to shells C11 and C12. The local deformations near the cutout in shell C13 are characterized by an ellipse-shaped inward buckle, which is in contrast to the deformation response near the cutout in shell C10 (the corresponding shell with 0º-ply reinforcement configuration) that has large magnitude outward radial deformations near the cutout. In addition, the attenuation length of the shell-wall deformations increases, and large magnitude radial deformations develop in a large portion of the shell away from the cutout. In particular, large ellipse-shaped inward buckles develop in the bending boundary layer region of the shell (see **X** symbols in Fig. 7c). In addition, the magnitude of the normalized shell-wall deformations decrease significantly to

between -0.37 to 0.45 for shell C13, and correspond to a 43% decrease in the magnitude of the deformations near the cutout compared to shell C1. In general, these results indicate that the character and magnitudes of the deformation responses for shells with 4.4-in-square 90º-ply reinforcement (see Figs. 7a-7c) can be significantly different from the corresponding shells with 0º-ply reinforcement (see Figs. 6a-6c). In particular, the 0º-ply reinforcement in shells C8-C10 reduces the local deformations near the cutout just before buckling. In contrast, shells C11-C13 can exhibit increases in the local deformations with an increase in the reinforcement thickness.

The character of the local axial and circumferential stress resultant distributions near the cutout just before buckling for shells C11 and C12 is similar to that of shell C1 shown in Fig. 4a. However, the magnitudes of the stress resultants can be significantly different. The magnitudes of the axial and circumferential stress resultant components in the regions of biaxial compression near the cutout just before buckling are as follows: N_x = -681 lb/in. and N_θ = -126 lb/in. for shell C11, and N_x = -843 lb/in. and N_θ = -173 lb/in. for shell C12, compared to N_x = -568 lb/in. and N_θ = -110 lb/in. for shell C1. The regions of biaxial compression are marked with an **X** symbol in Fig. 7. These results correspond to axial stress concentration factors equal to 1.26 and 1.30 (1.31 for shell C1) and biaxial-stress ratios of 0.19 and 0.21, for shells C11 and C12, respectively (0.19 for shell C1). The magnitudes of the axial stress concentration factor and the biaxial-stress ratio for these shells are approximately 7.2% less and 21% greater, respectively, than the axial stress concentration factors and the bi-axial stress ratio for the corresponding shells with 0o reinforcement configuration (shells C8-C9). In contrast, the axial and circumferential stress resultant distributions change significantly as the thickness of the reinforcement configuration increases further to 0.02 inches. Specifically, shell C13 has localized regions of in-plane biaxial compression stress resultants in the bending boundary layer region of the shell and the magnitudes of the stress resultants are N_x = -838 lb/in. and N_θ = -128 lb/in., which correspond to an axial stress concentration factor of 1.08, and a biaxial-stress ratio of 0.15. This response characteristic is similar to that of the corresponding shell C10 with 0º-ply reinforcement configuration. The results also indicate that shells C11-C13 with 0º-ply reinforcement exhibit similar post-local-buckling and collapse response trends as those of the corresponding shells C8-C10 with 0º reinforcement configurations. Specifically, shells C11 and C12 have a local buckling response near the cutout and this local buckling response causes global collapse to occur immediately after the local instability occurs. However, as the reinforcement thickness is increased, e.g., shell C13, the shell no longer has a local buckling response near the cutout, rather, a local buckling response occurs in the bending boundary layer region of the shell, and this local buckling response causes the global collapse of the shell.

Response Trends Results illustrating the effects of cutout reinforcement area, thickness, and ply orientation on the local buckling load of a shell with a cutout are presented in Fig. 8. The buckling load of the shell, P_{cr}, is normalized by the buckling load of the corresponding shell with no cutout, $P_{cr}{}^{o}$, predicted from a linear bifurcation analysis. The solid and dashed lines correspond to results for shells with 0º- and 90º-ply cutout reinforcement configurations, respectively. The results indicate that, in all cases, the buckling load of the shell increases as the reinforcement thickness increases. In addition, the results indicate that, in general, the buckling load of a shell with a 90º-ply cutout reinforcement configuration is greater than the buckling load of the corresponding shell with a 0º-ply reinforcement configuration. The results also indicate that the effects of reinforcement ply orientation become more pronounced as the size or area of the reinforcement increases. Shells with a 2.4-in.-square cutout reinforcement configuration exhibit a small variation in the buckling load with a variation in the reinforcement ply orientation. However, as the area of the reinforcement increases, the difference in the buckling load of a shell for a given reinforcement thickness, can be as large as 25%. The results indicate that the buckling load of a shell with a 90º-ply reinforcement configuration increases as the area of the reinforcement configuration increase. Similarly, the buckling load of a shell with a 0º-ply reinforcement

configuration increases as the area of the reinforcement configuration increase from a 2.4- to a 4.4-in.-square reinforcement configuration. However, a further increase in the area of the reinforcement configuration to 8.0-in-square causes a reduction in the buckling load of the shell.

A comparison of predicted local buckling loads as a function of the ratio of cutout reinforcement volume, V_r, to the nominal shell volume, V_s, is presented in Fig. 9. The solid and dashed lines correspond to results for shells with 0º- and 90º-ply cutout reinforcement configurations, respectively. The results indicate that shells with 2.4-in.-square cutout reinforcement configurations have the greatest increase in buckling load for the smallest increase in structural volume, followed by shells with 4.4-in.-square reinforcement configurations, and then shells with 8.0-in.-square reinforcement configurations. In particular, shells with 2.4-in.-square reinforcement configurations have a 48% increase in the buckling load with only a 0.3% increase in structural volume. Shells with 4.4-in.-square reinforcement configurations require a 0.6% to 0.8% increase in the structural volume to achieve a similar improvement in the buckling load for a given reinforcement ply orientation. Similarly, shells with 90º-ply, 8.0-in.-square cutout reinforcement configurations require a 1.75% increase in structural volume to achieve a similar improvement in the buckling load. However, the shells with the 0º-ply, 8.0-in.-square cutout reinforcement configurations do not achieve a similar increase in buckling load achieved by the shells with smaller reinforcement configurations.

Anomalous Behavior Results presented in the previous section indicate that, in general, the buckling load of a shell with a cutout increases with an increase in the reinforcement size. However, the shells C14-C16 with 8.0-in.-square, 0º-ply cutout reinforcement configurations have buckling loads than the corresponding shells with smaller 4.4-in.-square cutout reinforcement configurations (see Fig. 8). Most notably, shell C16, with a four-ply-thick reinforcement configuration, has a normalized buckling load equal to 0.74 compared to 0.78 and 0.84 for the corresponding shells with a 2.4-in.-square reinforcement configuration (shell C4) and a 4.4-in.-square reinforcement configuration (shell C10), respectively (see Fig. 8). Furthermore, the results indicate that, in the shells with an 8.0-in-square cutout reinforcement, a significant amount of the axial load in the shells is redistributed to the reinforced region of the shell near the cutout. This load redistribution results in substantially larger magnitude stress concentrations near the cutout than in the corresponding shells with smaller reinforcements (see Fig.10). In shells C14 and C15, these greater magnitude stresses couple with the local deformations near the cutout and cause the local buckling response to occur near the cutout at lower applied loads. The internal load distribution in shell C16 causes high magnitude destabilizing stresses and deformations to occur in the bending boundary layer region of the shell at lower applied loads, as shown in Fig. 10. The locations where buckling initiates are marked by X symbols in the figure. It is hypothesized that the formation of the large magnitude radial deformations in the bending boundary layer region of shell C16 is compounded by the interaction of non-attenuating bending boundary layers associated with the shell ends and the cutout reinforcement. The coupling of these localized stresses and deformations in the bending boundary layer regions of shell C16 ultimately causes the buckling of the shell in the bending boundary layer regions at a significantly lower applied load than the corresponding shells with smaller reinforcement.

Concluding Remarks

Results from a numerical study of the response of thin-wall compression-loaded quasi-isotropic laminated composite cylindrical shells with reinforced and unreinforced square cutouts have been presented. The results identify some of the effects of cutout-reinforcement orthotropy, size, and thickness on the nonlinear response of the shells. A high-fidelity nonlinear analysis procedure has been used to predict the nonlinear response of the shells.

The results presented herein indicate that a compression-loaded shell with an unreinforced cutout can exhibit a complex nonlinear response that is not typically found in the corresponding shell without a cutout. In particular, a local buckling response occurs in the shell that is caused by a localized nonlinear coupling between local shell-wall deformations and in-plane destabilizing compression stresses near the cutout. In general, the addition of reinforcement around a cutout in a compression-loaded shell can have a significant effect on the shell response. Results have been presented that indicate that the reinforcement can affect the local deformations and stresses near the cutout and retard or suppress the onset of local buckling in the shell near the cutout. For some cases, the local buckling response near the cutout in the shell results in a stable postbuckling response near the cutout and additional load can be applied to the shell before it undergoes a global collapse. For other cases, the local response near the cutout in the shell causes a disturbance of sufficient magnitude in the shell to cause global collapse to occur immediately after the local instability occurs. For still other cases, the reinforcement suppresses the local buckling response near the cutout and causes buckling to occur in the bending boundary layer regions near the ends of the shell. In general, the buckling load of the shell increases as the size and the thickness of the cutout reinforcement increases. However, some results indicate that in shells with a larger 0º-ply reinforcement, internal load redistribution can cause high magnitude destabilizing stresses and deformations to occur in the bending boundary layer region of the shell at lower applied loads than in the corresponding shell with small reinforcement. In addition, the results suggest that the formation of the large magnitude radial deformations in the bending boundary layer region of a shell can be compounded by the interaction of non-attenuating bending boundary layers associated with the shell ends and the cutout reinforcement. The coupling of these localized stresses and deformations in the bending boundary layer regions of the shell ultimately causes the buckling of the shell in the bending boundary layer regions at a significantly lower applied load. The results indicate that shells with 90º-ply cutout reinforcement generally have greater buckling loads than the corresponding shells with 0º-ply reinforcement. The results suggest that shells with the 90º-ply reinforcement achieve higher buckling loads because the shells with 90º-ply reinforcement exhibit smaller-magnitude axial-stress concentrations. In contrast, shells with 0º-ply reinforcement exhibit larger-magnitude axial-stress concentrations near the cutout.

The selected results presented herein suggest that tailoring the orthotropy, thickness and size of a cutout reinforcement in a compression-loaded shell and can result in significant increases in the buckling load of the shell, and can reduce the local deformations and stresses near the cutout. The results also suggest that a nonlinear analysis may be necessary to accurately characterize the complex nonlinear behavior exhibited by these structures. A robust high-fidelity nonlinear analysis procedure was used in the study and offers the opportunity to provide insight into the effects of various cutout reinforcement concepts on the response of compression-loaded shell structures. Moreover, results from such a high-fidelity analysis procedure can improve some of the engineering approximations and methods that are used in the design of reinforced cutouts in shell structures.

References

1. Lur'e, A. I., “Statics of Thin-walled Elastic Shells," State Publishing House of Technical and Theoretical Literature, Moscow, 1947; translation, AEC-tr-3798, Atomic Energy Commission, 1959.

2. Lekkerkerker, J. G., “On the Stress Distribution in Cylindrical Shells Weakened by a Circular Hole," Ph.D. Dissertation, Technological University, Delft, The Netherlands, 1965.

3. Brogan, F. A. and Almroth, B. O., “Buckling of Cylinders with Cutouts," AIAA Journal, Vol. 8, No. 2, February 1970, pp. 236-240.

4. Tennyson, R. C., “The Effects of Unreinforced Circular Cutouts on the Buckling of Circular Cylindrical Shells," Journal of Engineering for Industry, Transactions of the American Society of Mechanical Engineers, Vol. 90, November 1968, pp. 541-546.

5. Starnes, J. H., “The Effect of a Circular Hole on the Buckling of Cylindrical Shells," Ph. D. Dissertation, California Institute of Technology, Pasadena, CA, 1970.

6. Hilburger, M. W., Starnes, J. H., Jr., and Waas, A. M. "A Numerical and Experimental Study of the Response of Selected Compression-loaded Composite Shells with Cutouts," Proceedings of the 39th AIAA/ASME/ASCE/AHS/ASC Structures, Structural Dynamics, and Materials Conference, Long Beach, CA., AIAA Paper No. 98-1768, 1998.

7. Starnes, J. H., Jr., Hilburger, M. W., and Nemeth, M. P., "The Effects of Initial Imperfections on the Buckling of Composite Shells," Composite Structures: Theory and Practice, ASTM STP 1383, P. Grant and C. Q. Rousseau, Eds., American Society for Testing and Materials, 2000, pp. 529-550.

8. Almroth, B. O. and Holmes, A. M. C., "Buckling of Shells with Cutouts, Experiment and Analysis," International Journal of Solids and Structures, Vol. 8, August 1972, pp.1057-1071.

9. Cervantes, J. A. and Palazotto, A. N., "Cutout Reinforcement of Stiffened Cylindrical Shells," Journal of Aircraft, Vol. 16, March 1979, pp. 203-208.

10. Toda, S., "Buckling of Cylinders with Cutouts Under Axial Compression," Experimental Mechanics, pp. 414-417, December 1983.

11. Kuhn, P., Stresses in Aircraft and Shell Structures, McGraw-Hill Book Company, New York, 1956.

12. Hilburger, M. H., and Starnes, J. H., Jr., "Effects of Imperfections on the Buckling Response of Compression-loaded Composite Shells," International Journal of Non-linear Mechanics, Vol. 37, pp. 623-643, 2002.

13. Rankin, C. C., Brogan, F. A., Loden, W. A., and Cabiness, H. D., "STAGS Users Manual, Version 4.0," Lockheed Martin Missiles & Space Co., Inc., Advanced Technology Center, Report LMSC P032594, 1999.

14. Riks, E., "Progress in Collapse Analysis," Journal of Pressure Vessel Technology, Vol. 109, pp. 27-41, 1987.

15. Park, K. C., "An Improved Stiffly Stable Method for Direct Integration of Nonlinear Structural Dynamics," Journal of Applied Mechanics, Vol. 42, pp. 464-470, June 1975.

16. Riks, E., Rankin, C. C., and Brogan, F. A., "On the Solution of Mode Jumping Phenomena in Thin-walled Shell Structures," Computer Methods in Applied Mechanics and Engineering, Vol. 136 (1-2), pp. 59-92, 1996.

Table 1: Shell configurations

Shell identification code	Reinforcement size, in. x in.	Reinforcement ply orientation, deg.	Reinforcement thickness, in. (# of plies)
C1	-	-	-
C2	2.4 x 2.4	0	.005 (1)
C3	2.4 x 2.4	0	.01 (2)
C4	2.4 x 2.4	0	.02 (4)
C5	2.4 x 2.4	90	.005 (1)
C6	2.4 x 2.4	90	.01 (2)
C7	2.4 x 2.4	90	.02 (4)
C8	4.4 x 4.4	0	.005 (1)
C9	4.4 x 4.4	0	.01 (2)
C10	4.4 x 4.4	0	.02 (4)
C11	4.4 x 4.4	90	.005 (1)
C12	4.4 x 4.4	90	.01 (2)
C13	4.4 x 4.4	90	.02 (4)
C14	8.0 x 8.0	0	.005 (1)
C15	8.0 x 8.0	0	.01 (2)
C16	8.0 x 8.0	0	.02 (4)
C17	8.0 x 8.0	90	.005 (1)
C18	8.0 x 8.0	90	.01 (2)
C19	8.0 x 8.0	90	.02 (4)

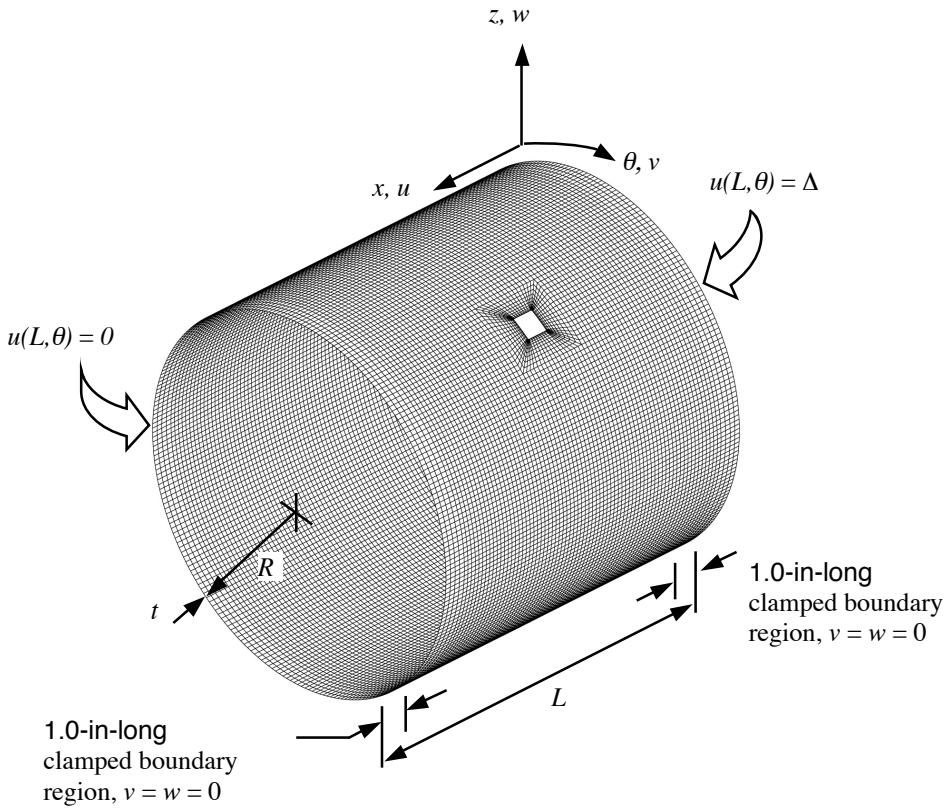

Fig. 1. Typical finite-element model geometry and boundary conditions.

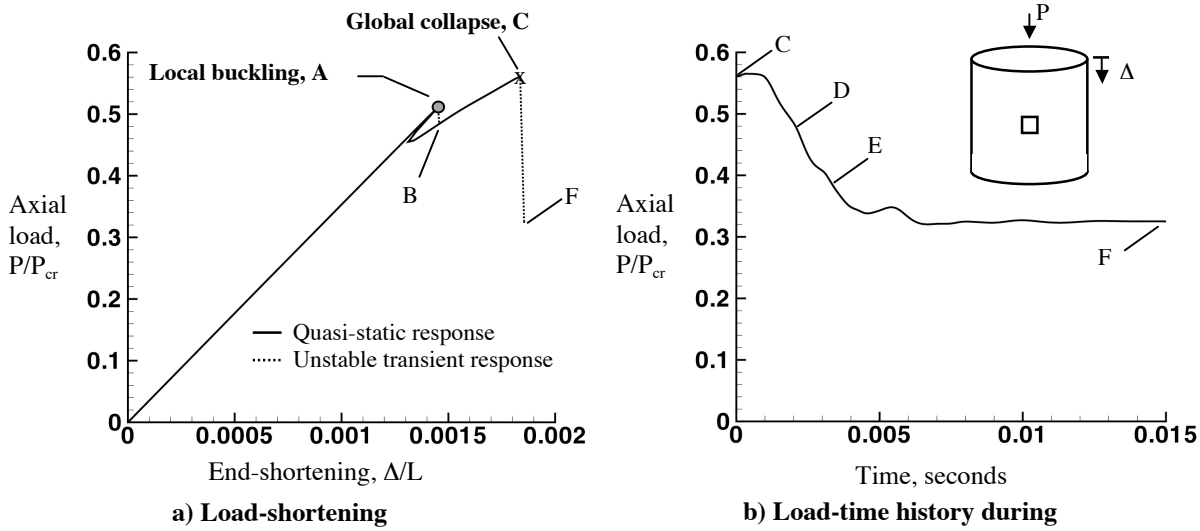

a) Load-shortening **b) Load-time history during**

Fig. 2. Numerically predicted nonlinear response of a compression-loaded cylindrical shell with an unreinforced cutout (shell C1).

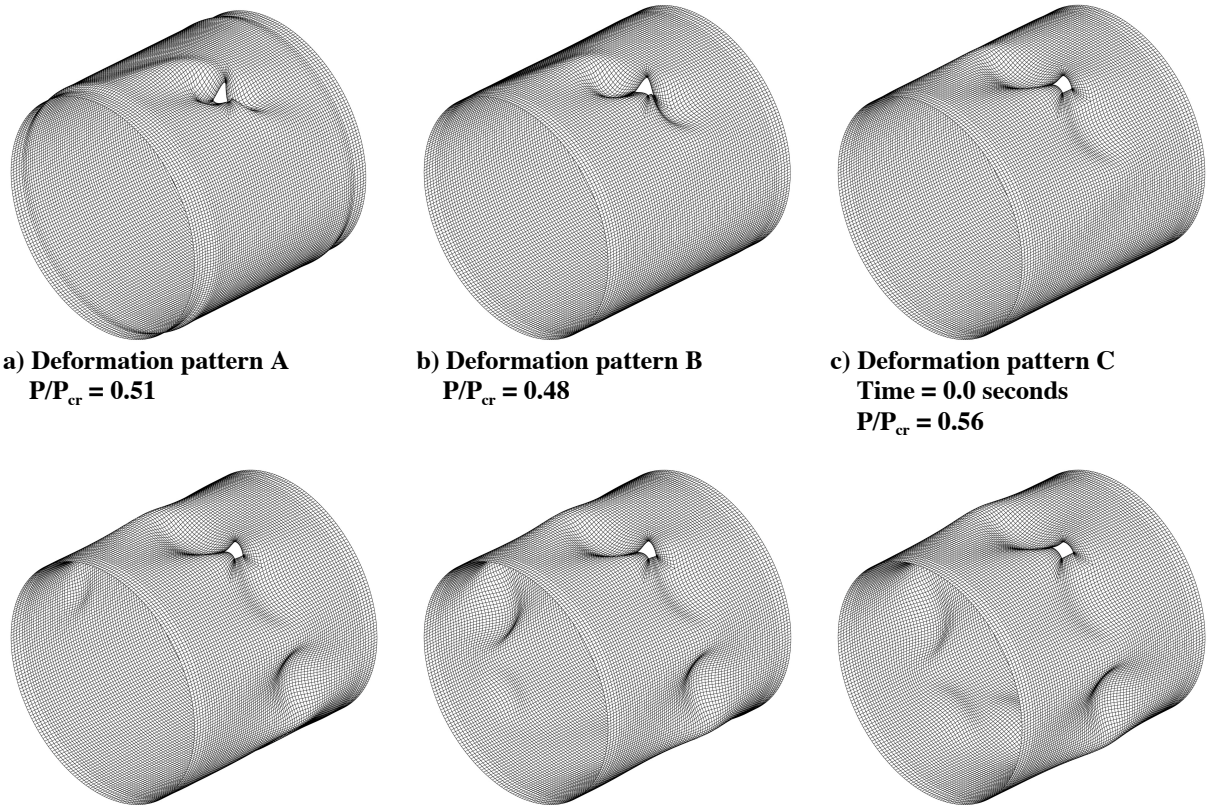

a) Deformation pattern A
P/P_{cr} = 0.51

b) Deformation pattern B
P/P_{cr} = 0.48

c) Deformation pattern C
Time = 0.0 seconds
P/P_{cr} = 0.56

d) Deformation pattern D
Time = 0.0022 seconds
P/P_{cr} = 0.47

e) Deformation pattern E
Time = 0.0035 seconds
P/P_{cr} = 0.39

f) Deformation pattern F
Time = 0.015 seconds
P/P_{cr} = 0.33

Fig. 3. Numerically predicted deformation response of a compression-loaded cylindrical shell with an unreinforced cutout (shell C1). The deformation patterns A-F correspond to the points labeled in Fig. 2.

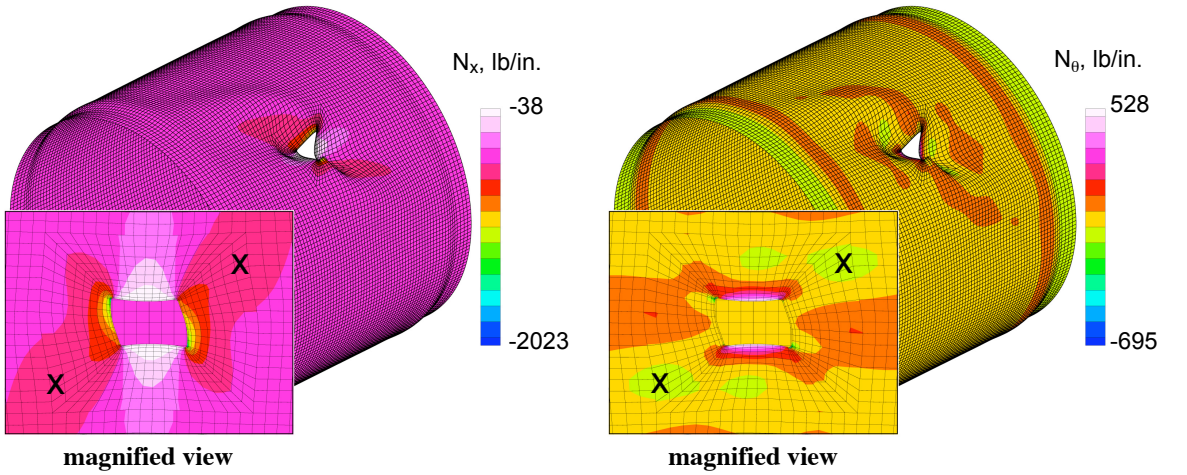

a) Initial local buckling, corresponding to Point A in Fig 2a, P/P_{cr} = 0.51

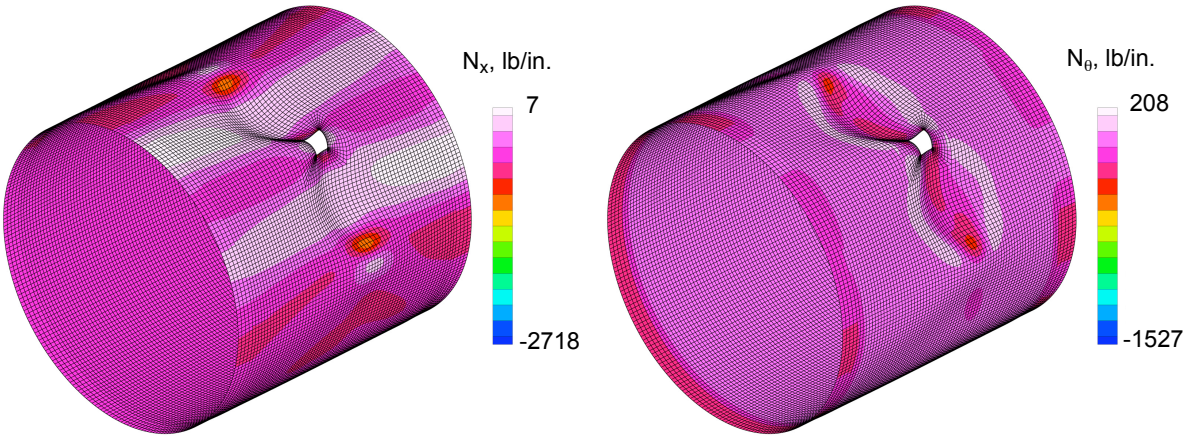

b) Initial global collapse, corresponding to Point C in Fig 2a, P/P_{cr} = 0.56, time = 0.0 seconds

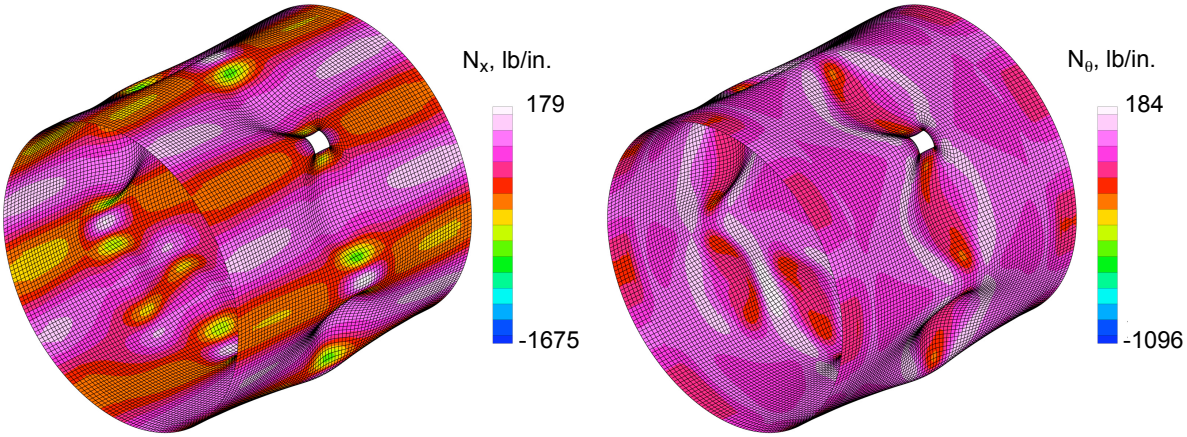

b) Post collapse, corresponding to Point F in Fig 2a, P/P_{cr} = 0.33, time = 0.015 seconds

Fig. 4. Numerically predicted deformation response and stress resultant contours at selected points in the nonlinear response of a compression-loaded cylindrical shell with an unreinforced cutout (shell C1).

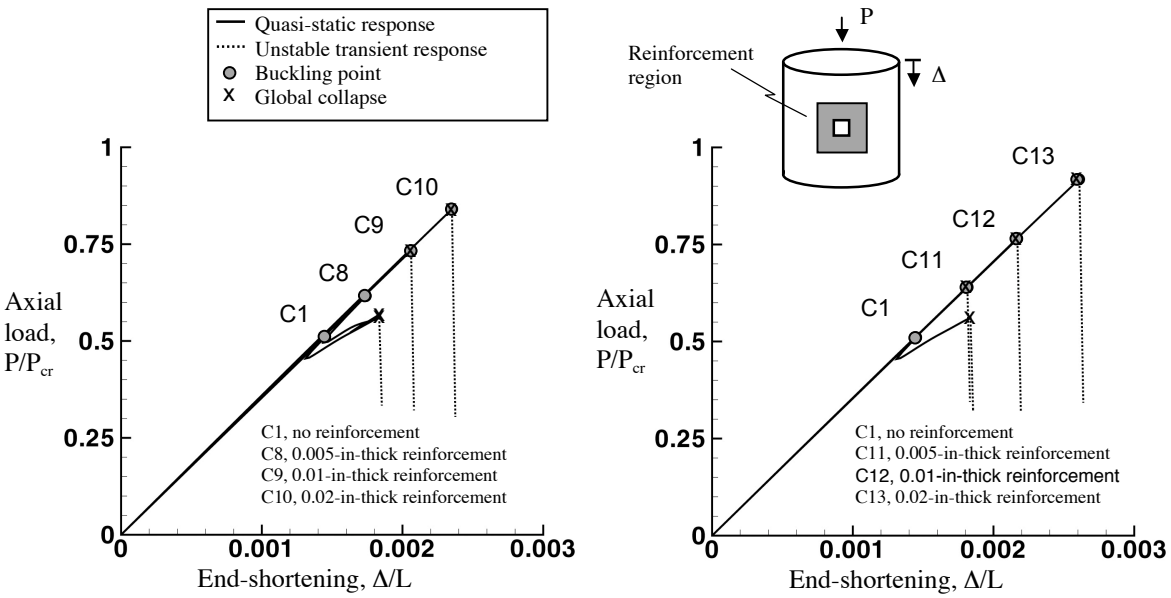

Fig. 5. Effects of cutout-reinforcement thickness and reinforcement fiber orientation on the predicted load-shortening response of a geometrically perfect compression-loaded cylindrical shell with a cutout (4.4-in square-shaped reinforcement).

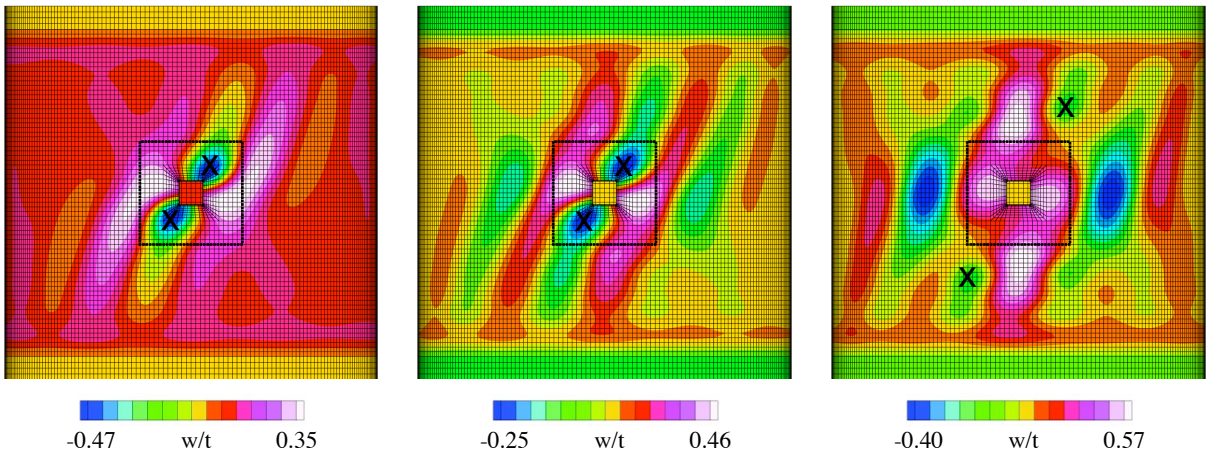

Fig. 6 Effects of cutout-reinforcement thickness on the predicted initial-buckling deformations of a geometrically perfect compression-loaded cylindrical shell with a cutout. The reinforcement is a 4.4-in. square-shaped reinforcement with 0°-ply orientation (the outer boundary of reinforcement region is marked in the figures).

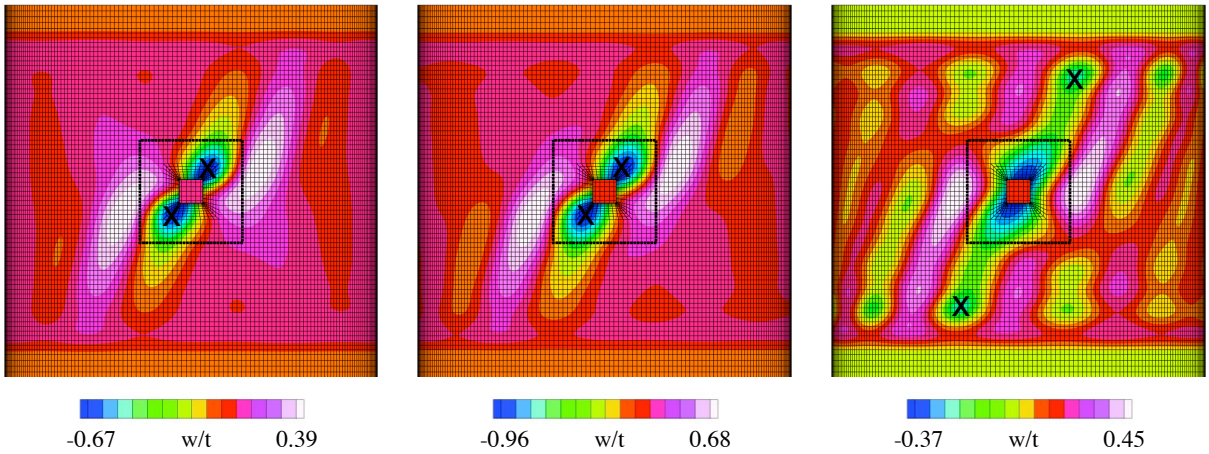

a) Shell C11, 0.005-in-thick reinforcement

b) Shell C12, 0.01-in-thick reinforcement

c) Shell C13, 0.02-in-thick reinforcement

Fig. 7. Effects of cutout-reinforcement thickness on the predicted initial-buckling deformations of a geometrically perfect compression-loaded cylindrical shell with a cutout. The reinforcement is a 4.4-in. square-shaped reinforcement with 90°-ply orientation (the outer boundary of reinforcement region is marked in the figures).

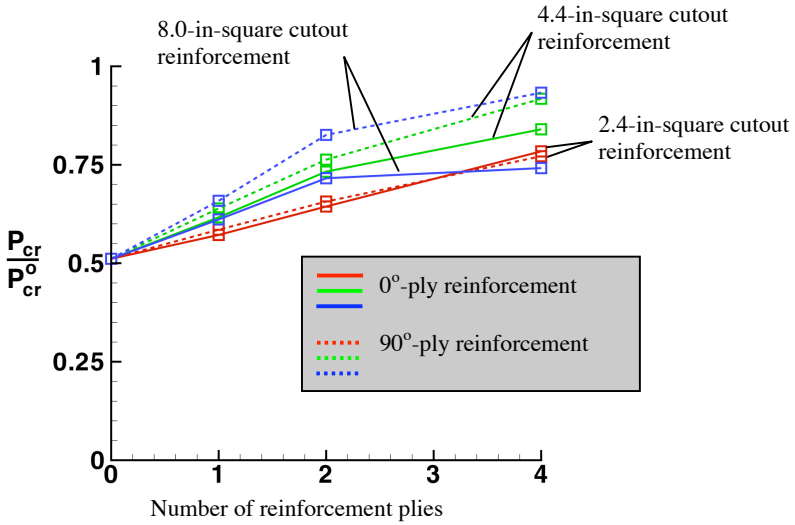

Fig. 8. The effects of cutout reinforcement configuration on the local buckling load of a geometrically perfect compression-loaded composite shell with a reinforced cutout.

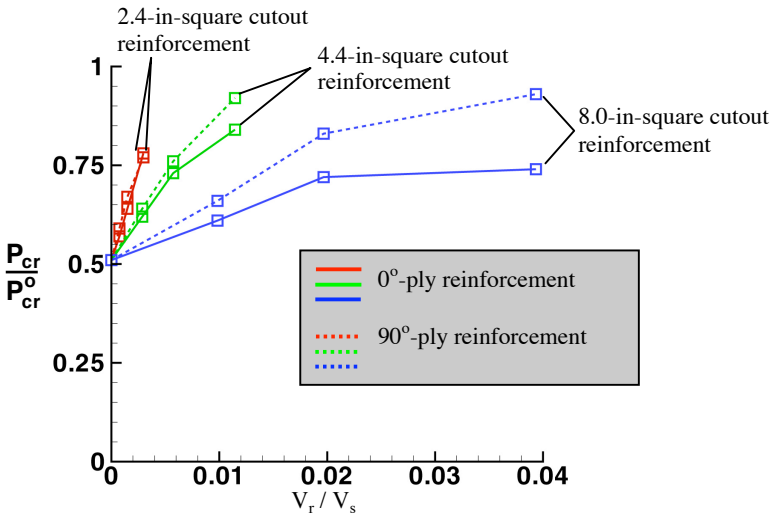

Fig. 9. Normalized local buckling load versus normalized cutout reinforcement volume for a geometrically perfect compression-loaded shell with a reinforced cutout.

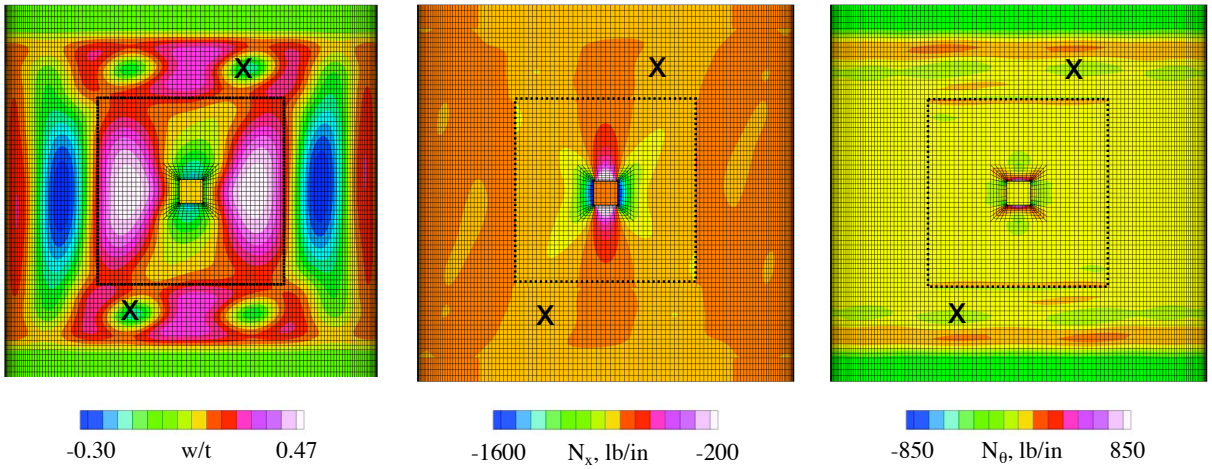

a) Radial deformation pattern

b) Axial stress resultant pattern

c) Circumferential stress resultant pattern

Fig. 10. Predicted radial deformation pattern and stress resultant patterns for a compression-loaded shell with an 8.0-in-square, 4-ply-thick, 0°-ply cutout reinforcement (the outer boundary of reinforcement region is marked in the figures).

REPORT DOCUMENTATION PAGE

Form Approved
OMB No. 0704-0188

1. REPORT DATE *(DD-MM-YYYY)*	2. REPORT TYPE	3. DATES COVERED *(From - To)*
01- 09 - 2004	Tecnical Memorandum	

4. TITLE AND SUBTITLE

Buckling Behavior of Compression-Loaded Composite Cylindrical Shells With Reinforced Cutouts

5a. CONTRACT NUMBER

5b. GRANT NUMBER

5c. PROGRAM ELEMENT NUMBER

6. AUTHOR(S)

Hilburger, Mark W.; and Starnes, James H., Jr.

5d. PROJECT NUMBER

5e. TASK NUMBER

5f. WORK UNIT NUMBER

23-719-20-30

7. PERFORMING ORGANIZATION NAME(S) AND ADDRESS(ES)

NASA Langley Research Center
Hampton, VA 23681-2199

8. PERFORMING ORGANIZATION REPORT NUMBER

L-19009

9. SPONSORING/MONITORING AGENCY NAME(S) AND ADDRESS(ES)

National Aeronautics and Space Administration
Washington, DC 20546-0001

10. SPONSOR/MONITOR'S ACRONYM(S)

NASA

11. SPONSOR/MONITOR'S REPORT NUMBER(S)

NASA/TM-2004-212656

12. DISTRIBUTION/AVAILABILITY STATEMENT

Unclassified - Unlimited
Subject Category 39
Availability: NASA CASI (301) 621-0390 Distribution: Standard

13. SUPPLEMENTARY NOTES

An electronic version can be found at http://techreports.larc.nasa.gov/ltrs/ or http://ntrs.nasa.gov
Paper presented at the 43st AIAA/ASME/ASCE/AHS/ASC Structures, Structural Dynamics, and Materials Conference, Denver, CO, April, 2002.

14. ABSTRACT

Results from a numerical study of the response of thin-walled compression-loaded quasi-isotropic laminated composite cylindrical shells with unreinforced and reinforced square cutouts are presented. The effects of cutout reinforcement orthotropy, size, and thickness on the nonlinear response of the shells are described. A nonlinear analysis procedure has been used to predict the nonlinear response of the shells. The results indicate that a local buckling response occurs in the shell near the cutout when subjected to load and is caused by a nonlinear coupling between local shell-wall deformations and in-plane destabilizing compression stresses near the cutout. In general, reinforcement around a cutout in a compression-loaded shell is shown to retard or eliminate the local buckling response near the cutout and increase the buckling load of the shell. However, some results show that certain reinforcement configurations can cause an unexpected increase in the magnitude of local deformations and stresses in the shell and cause a reduction in the buckling load. Specific cases are presented that suggest that the orthotropy, thickness, and size of a cutout reinforcement in a shell can be tailored to achieve improved buckling response characteristics.

15. SUBJECT TERMS

Shell Buckling; Cutouts; Reinforcement

16. SECURITY CLASSIFICATION OF:			17. LIMITATION OF ABSTRACT	18. NUMBER OF PAGES	19a. NAME OF RESPONSIBLE PERSON
a. REPORT	b. ABSTRACT	c. THIS PAGE			STI Help Desk (email: help@sti.nasa.gov)
					19b. TELEPHONE NUMBER *(Include area code)*
U	U	U	UU	25	(301) 621-0390